nature chemical biology

Reconstitution of ThiC in thiamine pyrimidine biosynthesis expands the radical SAM superfamily

Abhishek Chatterjee[1,4], Yue Li[1,4], Yang Zhang[1], Tyler L Grove[2], Michael Lee[3], Carsten Krebs[2,3], Squire J Booker[2,3], Tadhg P Begley[1] & Steven E Ealick[1]

4-Amino-5-hydroxymethyl-2-methylpyrimidine phosphate (HMP-P) synthase catalyzes a complex rearrangement of 5-aminoimidazole ribonucleotide (AIR) to form HMP-P, the pyrimidine moiety of thiamine phosphate. We determined the three-dimensional structures of HMP-P synthase and its complexes with the product HMP-P and a substrate analog imidazole ribotide. The structure of HMP-P synthase reveals a homodimer in which each protomer comprises three domains: an N-terminal domain with a novel fold, a central $(\beta\alpha)_8$ barrel and a disordered C-terminal domain that contains a conserved CX_2CX_4C motif, which is suggestive of a [4Fe-4S] cluster. Biochemical studies have confirmed that HMP-P synthase is iron sulfur cluster–dependent, that it is a new member of the radical SAM superfamily and that HMP-P and 5′-deoxyadenosine are products of the reaction. Mössbauer and EPR spectroscopy confirm the presence of one [4Fe-4S] cluster. Structural comparisons reveal that HMP-P synthase is homologous to a group of adenosylcobalamin radical enzymes. This similarity supports an evolutionary relationship between these two superfamilies.

Thiamine pyrophosphate (ThDP, **1**) is an essential cofactor in all forms of life and has a key role in carbohydrate and amino acid metabolism[1]. The biosynthesis of ThDP has been extensively studied in prokaryotes and involves the separate formation of 4-methyl-5-β-hydroxyethylthiazole phosphate (thiazole phosphate, TMP, **2**) and 4-amino-5-hydroxymethyl-2-methylpyrimidine pyrophosphate (HMP-PP, **3**) (**Fig. 1a**)[1,2]. These are then coupled to form thiamine monophosphate (ThMP, **4**). A final phosphorylation gives ThDP, the biologically active form of the cofactor. The biosynthesis of ThDP in *Saccharomyces cerevisiae* uses a completely different biochemical pathway for which the details are just beginning to emerge[3–5].

The mechanistic enzymology of thiamine (**5**) thiazole (**2**) biosynthesis is now relatively well understood. The three identified pathways represented by *Escherichia coli*, *Bacillus subtilis* and *S. cerevisiae* have been reconstituted, and most of the required enzymes have been mechanistically and structurally characterized[2–6]. Biosynthesis of the thiamine thiazole in *E. coli* requires five gene products and uses 1-deoxy-D-xylulose 5-phosphate (DXP, **6**), tyrosine (**7**) and cysteine (**8**). The *B. subtilis* pathway is similar to that of *E. coli* but uses glycine (**9**) rather than tyrosine. Biosynthesis of the thiamine thiazole in yeast requires a single enzyme and uses nicotinamide adenine dinucleotide (NAD, **10**), glycine and an unknown sulfur source[4].

In contrast, very little is yet known about the mechanistic enzymology of thiamine pyrimidine (4-amino-5-hydroxymethyl-2-methylpyrimidine; HMP, **11**) formation; however, thiamine pyrimidine biosynthesis uses fundamentally different chemistry compared with that used for the biosynthesis of the nucleic acid pyrimidines. Labeling studies have established that HMP is derived from AIR (**12**) in bacteria (**Fig. 1b**)[7,8] and from histidine (**13**) and pyridoxal 5′-phosphate (PLP, **14**) in yeast (**Fig. 1c**)[9]. In each case, only a single gene is required for pyrimidine formation: *thiC* in bacteria, plants and algae, and *THI5* in yeast. Detailed studies, using isotopically labeled AIR, have established the origin of most of the atoms of HMP in bacteria (**Fig. 1b**). These studies were first carried out *in vivo* and later reproduced and expanded on using HMP-P (**15**) synthase in cell-free extract[7]. The labeling studies have established that the C2′ carbon of the ribose is reduced to the methyl oxidation state and used to methylate the C2 position on the aminoimidazole, and that the C4′ carbon of the ribose is inserted into the C4-C5 double bond of the aminoimidazole to generate the aminopyrimidine. The methyl hydrogens are derived from the C2′ hydrogen, the C3′ hydrogen and from the buffer. This rearrangement reaction is the most complex unresolved rearrangement in primary metabolism.

Radical *S*-adenosylmethionine (SAM, **16**) enzymes use SAM to generate a 5′-deoxyadenosyl radical (**17**) that in turn serves as an oxidant for a wide variety of enzymatic reactions[10,11]. For some enzymes, SAM is regenerated at the completion of the reaction, whereas for other enzymes SAM is a cosubstrate yielding 5′-deoxyadenosine (5-dAdo, **18**) as a product. Bioinformatic studies have identified more than 600 possible members of the radical SAM superfamily[12]. The radical SAM superfamily is characterized by a CX_3CX_2C motif that harbors a [4Fe-4S] cluster. Upon reduction,

[1]Department of Chemistry and Chemical Biology, 120 Baker Laboratory, Cornell University, Ithaca, New York 14853-1301, USA. [2]Department of Chemistry, 104 Chemistry Building, The Pennsylvania State University, University Park, Pennsylvania 16802, USA. [3]Department of Biochemistry and Molecular Biology, 108 Althouse Laboratory, The Pennsylvania State University, University Park, Pennsylvania 16802, USA. [4]These authors contributed equally to this work. Correspondence should be addressed to T.P.B. (tpb2@cornell.edu) or S.E.E. (see3@cornell.edu).

Received 1 August; accepted 23 September; published online 26 October 2008; doi:10.1038/nchembio.121

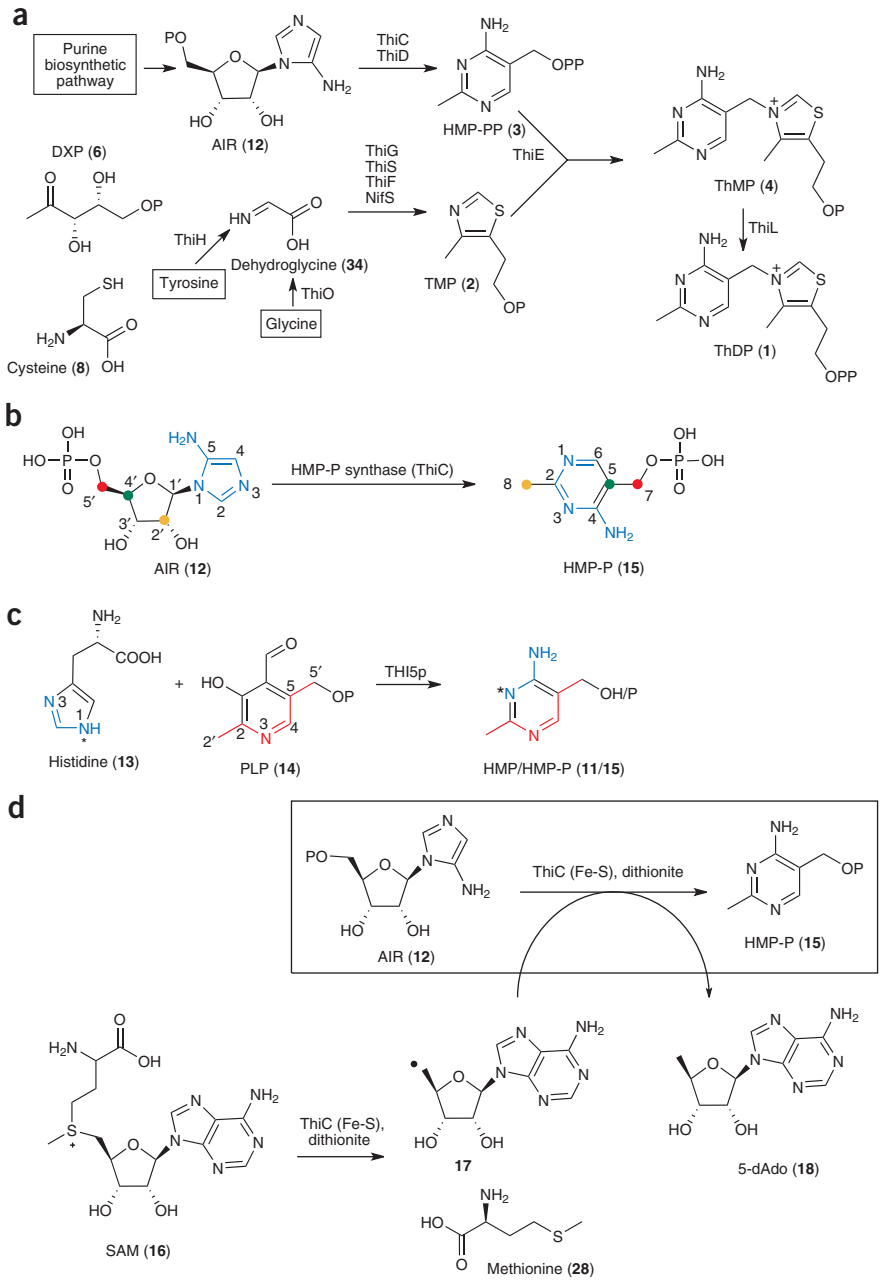

Figure 1 The biosynthesis of thiamine pyrophosphate. (**a**) Overall bacterial pathway. AIR (**12**) is converted to HMP-P (**15**) by HMP-P synthase (ThiC), which is phosphorylated by ThiD to give HMP pyrophosphate (**3**). The thiazole moiety (**2**) is biosynthesized from DXP (**6**), cysteine (**8**) and dehydroglycine (**34**). The dehydroglycine is generated from glycine (ThiO) in *B. subtilis* and from tyrosine (ThiH) in *E. coli*. The pyrimidine and thiazole are coupled by ThiE to give thiamine phosphate (**4**), and ThiL catalyzes the final phosphorylation. (**b**) Conversion of AIR to the thiamine pyrimidine in bacteria and plants. The color coding indicates the source of nonhydrogen atoms in HMP-P as demonstrated by labeling studies. (**c**) Biosynthesis of thiamine pyrimidine in fungi. In fungi the pyrimidine moiety is derived from histidine (**13**) and pyridoxal 5′-phosphate (**14**) using a single enzyme, THI5p. The color coding indicates the source of nonhydrogen atoms. (**d**) The HMP-P synthase reactions. When iron-sulfur cluster–loaded HMP-P synthase is reduced with dithionite, it reduces SAM (**16**) to generate methionine (**28**) and the 5′-deoxyadenosyl (5-dAdo) radical (**17**), which is required by HMP-P synthase to convert AIR to HMP-P.

the cluster serves as a source of an electron to produce the 5′-deoxyadenosyl radical.

Before our studies, HMP-P synthase, the *thiC* gene product, was not reported to be a radical SAM enzyme, although some evidence existed. Previous studies showed a conserved CX_2CX_4C motif in HMP-P synthase, and in *Salmonella enterica*, the C581A, C584A and C589A mutant proteins were unable to biosynthesize the thiamine pyrimidine, which suggested that HMP-P synthase contains an iron-sulfur cluster[13]. This possibility was further supported by the observation that iron-sulfur cluster biosynthetic mutants in *S. enterica* are thiamine requiring[13] and by a recent study demonstrating that HMP-P synthase from *Arabidopsis thaliana* purifies with a chromophore that is consistent with a bound iron-sulfur cluster[14].

In this paper, we report the first successful reconstitution of purified bacterial HMP-P synthase, demonstrate that the enzyme is a previously unrecognized radical SAM enzyme using SAM as a cosubstrate and producing HMP-P and 5′-deoxyadenosine as products, characterize the [4Fe-4S] cluster using Mössbauer and EPR spectroscopies, and describe structures of the enzyme complexed with a substrate analog and with the product, HMP-P.

RESULTS

Chemical reconstitution of HMP-P synthase

Cell-free extract from the *Caulobacter crescentus* HMP-P synthase–overexpressing *E. coli* strain was subjected to chemical Fe-S cluster reconstitution by the addition of excess Fe^{2+} and S^{2-} under strictly anaerobic conditions. After removal of the excess Fe(II) and S^{2-} by gel filtration, the resulting dark brown cell-free extract was fractionated, again under strictly anaerobic conditions, by nickel nitrilotriacetic acid affinity chromatography. The protein thus obtained was dark brown in color, with a UV-visible spectrum suggestive of the presence of an iron-sulfur cluster (**Figs. 1d** and **2a** and **Supplementary Fig. 1a** online). Analyses of bound iron and sulfide revealed 7.2 ± 0.3 irons and 5.4 ± 0.4 sulfides associated with each monomer.

Activity of chemically reconstituted HMP-P synthase

Thiamine pyrimidine formation was initially assayed using the thiochrome assay (**Supplementary Fig. 1b**). In this assay, the product of HMP-P synthase is converted to thiamine phosphate enzymatically. This is then oxidized to the intensely fluorescent thiochrome phosphate (**19**), which can be readily detected by HPLC analysis with fluorescence detection.

The results of this assay are shown in **Figure 2b**. The blue trace shows the HMP-P synthase activity in the iron-sulfur cluster-reconstituted cell-free extract. This activity is 14-fold higher than

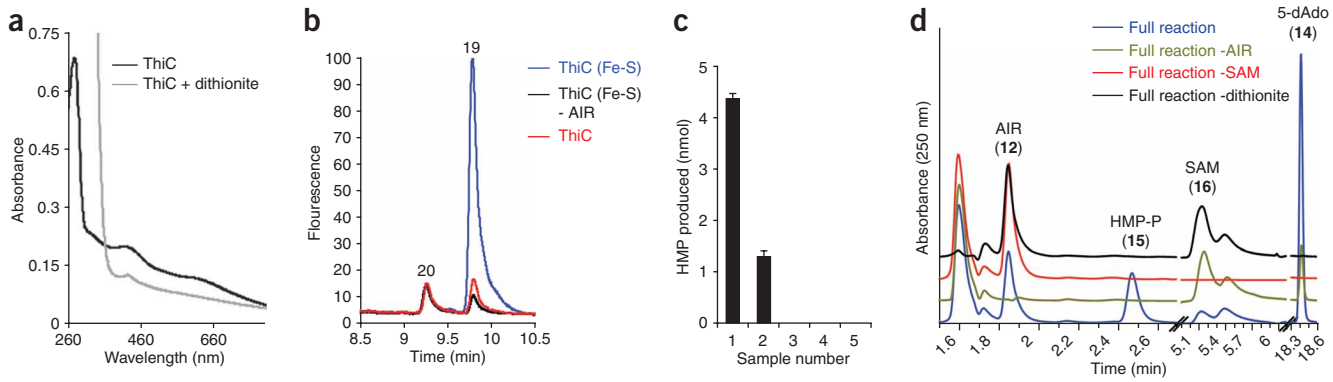

Figure 2 HMP-P synthase activity. (**a**) UV-visible absorption spectrum of isolated, iron-sulfur cluster–reconstituted HMP-P synthase (25 μM; black trace) and its change upon reduction with 200 μM dithionite (gray trace). (**b**) *In vitro* reconstitution of HMP-P biosynthesis, analyzed by HPLC after converting HMP-P to the fluorescent thiochrome phosphate (**19**). Enhanced product yield is observed when HMP-P synthase is subjected to chemical iron-sulfur cluster reconstitution. Blue and black traces represent reactions using iron-sulfur cluster–reconstituted and untreated HMP-P synthase lysate, respectively; red trace represents a reaction lacking AIR. The thiochrome pyrophosphate (**20**) peak arises from thiamine pyrophosphate in lysate and stays constant. (**c**) Activity of iron-sulfur cluster–reconstituted, purified HMP-P synthase. Sample 1 is reaction mixture containing HMP-P synthase, AIR, SAM and dithionite. Sample 2 is reaction 1 incubated aerobically. Samples 3, 4 and 5 are reaction 1 without SAM, AIR and dithionite, respectively. Error bars show s.d. (**d**) HPLC analysis of the HMP-P synthase reactions. Blue trace represents full reaction (HMP-P synthase, AIR, SAM and dithionite); green trace, red trace and black trace represent the full reaction without AIR, SAM and dithionite, respectively. Reaction products HMP-P (r_t = 2.58 min) and 5-dAdo (**18**) (r_t = 18.45 min) were identified by comigration with authentic standards and subsequent spectroscopic characterization. Three sections of the chromatogram (1.5–2.7 min, 5–6 min and 18.3–18.6 min) are presented to clearly demonstrate the changes.

the activity observed with untreated HMP-P synthase in cell-free extract (red trace) and supports the hypothesis that HMP-P synthase is an iron-sulfur cluster–using enzyme. The black trace shows the thiochrome phosphate present in the reconstituted sample in the absence of AIR. The thiochrome phosphate produced in this sample is due to the thiamine phosphate that copurifies with thiamine phosphate synthase[15]. The compound eluting at 9.3 min is thiochrome pyrophosphate (**20**) derived from enzyme-bound thiamine pyrophosphate in the cell-free extract. The concentration of this compound is the same in all three samples.

Similar activity of HMP-P synthase was also achieved using the purified protein. This activity was dependent on SAM, AIR and reduction of the iron-sulfur cluster using dithionite (**21**) (**Fig. 2c**). The purified enzyme was rapidly inactivated by exposure to air.

Identification of the HMP-P synthase reaction products

The thiochrome assay for detecting the formation of HMP is highly sensitive and was very useful in searching for optimized reconstitution conditions; however, it is an indirect assay and does not give information on the phosphorylation state of HMP. This is because HMP and HMP-P are both substrates for the pyrimidine kinase, and the phosphate is lost during thiamine formation[16]. In addition, we wished to determine the role SAM plays in this reaction. With the optimized reconstitution of the HMP-P synthase in a defined system, the available levels of activity allowed us to assay directly for the products without thiochrome derivatization.

A reaction mixture containing AIR, SAM, dithionite and HMP-P synthase was directly analyzed by HPLC with UV detection. The resulting chromatogram for the complete reaction (blue trace) shows consumption of AIR and SAM and the production of two new species with retention times of 2.58 and 18.45 min (**Fig. 2d**). These reaction products were identified as HMP-P and 5′-deoxyadenosine, respectively, by comigration with authentic standards. For further verification, ^{1}H NMR and ESI-MS analyses were performed on HPLC-purified products, which confirmed the structural assignments (**Supplementary Figs. 1c,d** and **2a** online). Control reactions lacking SAM and dithionite, run under identical reaction conditions, did not show the production of HMP-P or 5-dAdo. A reaction run in the absence of AIR shows reduced levels of 5-dAdo formation, which suggests that reduced levels of SAM reduction occur in the absence of AIR.

The reaction yield varied between protein preparations. Typically, 75–150 μM HMP-P and 200–450 μM 5-dAdo are produced in a reaction containing 0.8–1.2 mM isolated HMP-P synthase (depending on the yield of the corresponding enzyme purification), 400 μM AIR and 800 μM SAM. Notably, the production of 5-dAdo was consistently higher (approximately three-fold) than that of HMP-P, and the product yields were enzyme concentration–dependent (**Supplementary Fig. 2b**). Formation of HMP-P and 5-dAdo was very fast (**Supplementary Fig. 3a** online) and was essentially complete within mixing time (30 s).

In vivo reconstitution of HMP-P synthase

Co-expression of iron-sulfur clusters using proteins in *E. coli* containing the pDB1282 plasmid is an established strategy for the *in vivo* reconstitution of the cluster. This plasmid encodes a set of proteins involved in iron-sulfur cluster biogenesis (IscS, IscU, IscA, HscB, HscA and Fdx). Co-expression with pDB1282 substantially enhanced (four-fold) HMP-P synthase activity in cell-free extract over a control experiment in which HMP-P synthase was expressed in the absence of pDB1282 (**Supplementary Fig. 3b**). Anaerobic purification led to pure protein, with 3.8 ± 0.3 irons and 4.4 ± 0.6 sulfides per monomer (**Supplementary Fig. 3c**). When 195 μM protein was incubated anaerobically with 200 μM AIR, 400 μM SAM and 5 mM dithionite, production of 110 ± 20 μM HMP-P and 230 ± 11 μM 5-dAdo was observed (**Supplementary Fig. 4a** online).

Mössbauer spectroscopy

A sample of HMP-P synthase that was grown on medium supplemented with the Mössbauer-active isotope ^{57}Fe and isolated under strict anaerobic conditions contained only 1.7 irons and 1.2 sulfides per monomer. The Mössbauer spectrum (**Supplementary Fig. 4b**) reveals a quadrupole doublet with parameters typical of a [4Fe-4S]$^{2+}$

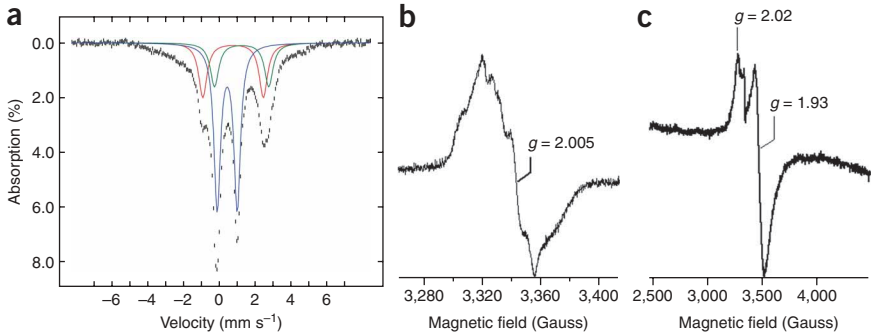

Figure 3 EPR and Mössbauer spectroscopy of HMP-P synthase. (**a**) 4.2-K/53-mT Mössbauer spectrum of a sample of HMP-P synthase overexpressed in bacteria grown on ^{57}Fe-supplemented medium and further reconstituted with ^{57}Fe, sulfide and DTT (hashed marks). The solid lines are simulations with three quadrupole doublets using the parameters quoted in the text, representing $[4Fe\text{-}4S]^{2+}$ clusters (blue), and two distinct high-spin Fe(II) species (red and green). (**b**) EPR spectrum of an as-isolated sample of HMP-P synthase that was coexpressed with Isc cluster. The spectrum is an average of 50 scans, which were obtained under the following conditions: microwave power, 6 μW; receiver gain, 60; modulation amplitude, 4 G; temperature, 20 K; microwave frequency, 9.4 GHz. (**c**) EPR spectrum of reconstituted HMP-P synthase. The sample (500 μM) was reduced with 10 mM dithionite before anaerobically loading into an EPR tube and freezing. The spectrum was obtained under the following conditions: microwave power, 101 μW; receiver gain, 30; modulation amplitude, 10 G; temperature, 13 K; microwave frequency, 9.5 GHz.

cluster. The remaining iron (two species) has parameters typical of high-spin Fe(II). We attribute the low stoichiometry (~0.2 $[4Fe\text{-}4S]^{2+}$ clusters per HMP-P synthase) to the rapid overexpression of HMP-P synthase despite the fact that the products of the *isc* genes from *Azotobacter vinelandii* were co-expressed. Therefore, we reconstituted anaerobically isolated HMP-P synthase with additional ^{57}Fe(II) and sulfide in the presence of DTT (22). This sample contained 7.2 irons and 5.4 sulfides per HMP-P synthase. The 4.2-K, 53-mT Mössbauer spectrum of this sample is shown (**Fig. 3a**, hashed marks). The spectrum is dominated by several well-resolved lines, in addition to a broad and featureless absorption, which ranges from –5 mm s^{-1} to +5 mm s^{-1} and accounts for ~30% of the total intensity. EPR spectroscopy of an identical sample reveals no signals attributable to iron-sulfur clusters with $S = 1/2$ ground state ($[3Fe\text{-}4S]^{+}$, $[4Fe\text{-}4S]^{+}$ and $[2Fe\text{-}2S]^{+}$), thereby ruling out the presence of these cluster types in this sample (*vide infra*). Consequently, the broad features are attributed to iron bound nonspecifically to HMP-P synthase[17]. The well-resolved lines can be simulated with three quadrupole doublets with the following parameters: $\delta_1 = 0.45$ mm s^{-1} and $\Delta E_{Q,1} = 1.12$ mm s^{-1} (43% of total intensity, 3.1 irons per HMP-P synthase, blue); $\delta_2 = 0.78$ mm s^{-1} and $\Delta E_{Q,2} = 3.37$ mm s^{-1} (18% of total intensity, 1.3 irons per HMP-P synthase, red); and $\delta_3 = 1.26$ mm s^{-1} and $\Delta E_{Q,3} = 3.02$ mm s^{-1} (14% of total intensity, 1.0 iron per HMP-P synthase, green). The parameters of the first quadrupole doublet are typical of $[4Fe\text{-}4S]^{2+}$ clusters, which suggests that reconstituted HMP-P synthase has ~0.8 $[4Fe\text{-}4S]^{2+}$. We therefore conclude that HMP-P synthase harbors one [4Fe-4S] cluster. The remaining two quadrupole doublets have parameters typical of Fe(II) in a four-coordinate, sulfur-rich environment (doublet 2) and a five- or six-coordinate environment of hard nitrogen/oxygen ligands (doublet 3)[18]. We speculate that one of the two Fe(II) species may be bound in the mononuclear $(His)_2$-ligated site that was identified from the X-ray structure (*vide infra*), but we cannot assign it without further knowledge of the coordination environment of the mononuclear site.

EPR spectroscopy

The electron paramagnetic resonance (EPR) spectrum of as-isolated HMP-P synthase is largely silent; however, a weak narrow signal is observed at $g = 2$ and is still present at 77 K, which suggests the presence of an organic radical (**Fig. 3b**). At present, the nature of this radical and its catalytic competence are unknown. Upon reduction of as-isolated or reconstituted HMP-P synthase in the presence of 10 mM dithionite, an axial spectrum emerges (**Fig. 3c**), displaying approximate g values of 2.02 and 1.93, which suggest a $[4Fe\text{-}4S]^{+}$ cluster. Consistent with this assignment, the spectrum substantially reduces in intensity at temperatures above 30 K and is nearly unobservable above 50 K. Spin quantification indicates that the spectrum accounts for less than 0.1 equivalent of spin per HMP-P synthase.

Structure of HMP-P synthase

The crystal structure of HMP-P synthase from *C. crescentus* was determined initially at 2.8 Å resolution. The overall structure is a homodimer with one dimer per asymmetric unit. Each protomer contains a bound metal ion, assigned as Zn(II) based on the peak height in difference electron density maps, and an HMP molecule, which in the beginning was thought to be a possible product and therefore added during crystallization. Each protomer consists of three domains (**Fig. 4a**). Domain 1 comprises the first 213 residues. This domain contains a novel fold consisting of six α-helices and five β-strands (**Supplementary Fig. 5a**,**b** online). The secondary structural elements form a thin blanket-like structure that folds over domains 2 and 3. Domain 2 comprises residues 214–510 and has a $(\beta\alpha)_8$ barrel fold in which β-strands 6–13 make up the barrel core. Each β-strand is followed by one α-helix except β8 (α9 and α10) and β9 (α11, α12, α13 and α14). The bottom of the barrel (N-terminal end of the β-strands) is covered by β-strands 1 and 2 of domain 1. Domain 3 comprises residues 511–548. These residues form an antiparallel three-helix bundle followed by a loop that extends into the top of the $(\beta\alpha)_8$ barrel of the adjacent protomer. The protein contains 76 additional C-terminal residues that are disordered in our structure. Two additional structures with different ligands and with resolutions of 2.0 Å were also determined. The complexes crystallized with a slightly smaller unit cell and did not contain the transition metal. All three structures showed the same general structural features with a disordered C terminus. Refinement statistics are given in **Supplementary Table 1** online.

The HMP-P synthase homodimer has approximate dimensions of 100 Å × 60 Å × 48 Å (**Fig. 4a**). Dimer formation joins the two $(\beta\alpha)_8$ barrels in an approximately antiparallel arrangement and buries a total of 2,800 $Å^2$ (12.6%) of solvent-accessible surface per monomer. The interface is mostly hydrophobic; 72.7% of the atoms are nonpolar. The main interactions involve helices α16, α17 and α18 (the last three helices in the $(\beta\alpha)_8$ barrel) and the three-helix bundle (α19, α20, α21) at the beginning of domain 3.

HMP-P synthase active site

The HMP-P synthase active site was identified using complexes with HMP-P and imidazole ribonucleotide (IMR, 23) (**Supplementary**

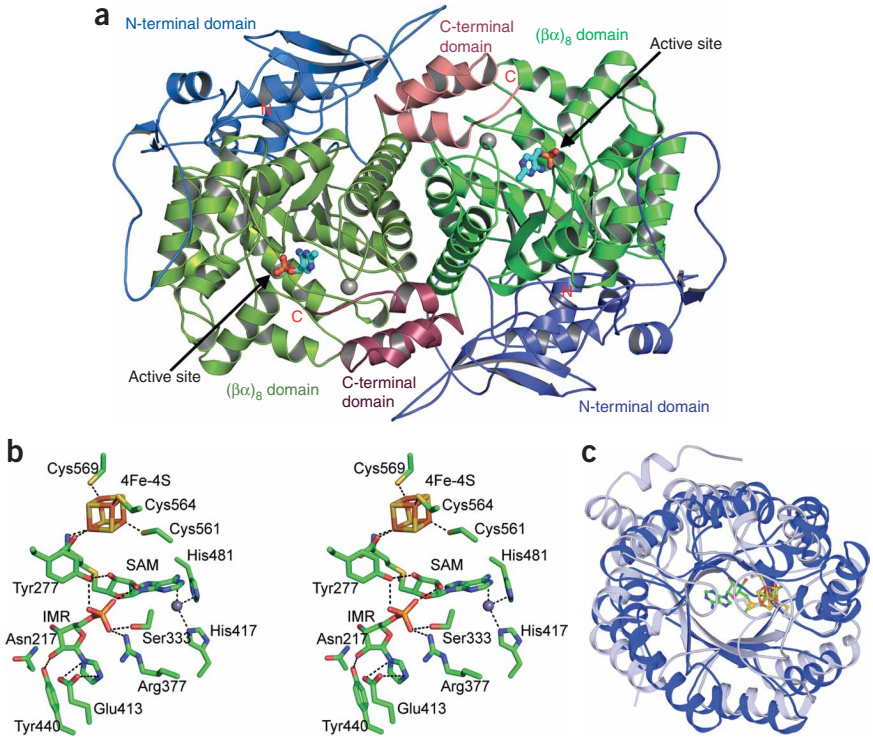

Figure 4 Structure of HMP-P synthase. (**a**) The HMP-P synthase homodimer. The protomer consists of three domains. The N-terminal domains are colored in shades of blue, the $(\beta\alpha)_8$ core domains are colored in shades of green and the C-terminal domains are colored in shades of red. HMP-P is shown as a ball-and-stick model. The final 66 amino acids are disordered; however, the final ordered residues, which immediately precede a conserved CX_2CX_4C motif, extend into the active site of the adjacent protomer. The C-terminal tail is anchored to the adjacent protomer by a three-helix bundle motif located at the beginning of the C-terminal domain. (**b**) Stereoview of the HMP-P synthase active site with modeled SAM and the [4Fe-4S] cluster. The atoms are color coded by atom type (green = C, blue = N, red = O, yellow = S and orange = Fe). The substrate analog IMR 22 from the crystal structure is shown. Residues Cys561, Cys564 and Cys569, SAM and the [4Fe-4S] cluster were modeled using biotin synthase as a guide. Hydrogen bonds are indicated by dotted lines. (**c**) Superposition of the $(\beta\alpha)_8$ domains from HMP-P synthase and biotin synthase (PDB ID 1R3O). HMP-P synthase is shown in blue, and biotin synthase is shown in silver. The [4Fe-4S] cluster and SAM from biotin synthase are shown as ball-and-stick models.

Fig. 5c–e). The active site is within a cavity at the C-terminal end of the $(\beta\alpha)_8$ barrel, with 1,300 Å^2 of solvent-accessible area and 1,900 Å^3 of solvent-accessible volume (**Fig. 4a**). Most of the residues in the active site cavity are highly conserved among the HMP-P synthase orthologs (**Supplementary Fig. 6** online). A large peak assigned as a Zn(II) with tetrahedral geometry is located within the active site and is coordinated by the Nε2 of His417, the Nε2 of His481 and two water molecules with unusually long distances (**Supplementary Fig. 7a,b** online). Though the identity of the transition metal remains uncertain, the *B*-factor obtained during refinement is consistent with an assignment of Zn(II).

The HMP-P site is located near the N terminus of helix α12 and the C terminus from the adjacent protomer. Hydrophobic residues Met248, Leu250, Val274 and Tyr440 line one side of the active site cavity. Atoms N1 and N2 of the pyrimidine moiety form hydrogen bonds with the side chains of Glu414 and Ser474, respectively, assuming that the former is protonated. The phosphate binding site is located at the N terminus of α12 and is stabilized by the helix dipole (**Supplementary Fig. 5e**). Hydrogen bonds form with the amide nitrogen atom of Gly335, Oη of Tyr277, Nε2 of His313, Oγ of Ser333 and Nη1 of Arg377.

The phosphate binding site of IMR is similar to that of HMP-P, and the imidazole and ribose moieties generally overlap the pyrimidine binding site of the HMP-P structure. Atom N3 of the imidazole ring forms a hydrogen bond with the side chain of Asp347, assuming that it is protonated. The two hydroxyl groups of the ribose moiety of IMR are hydrogen bonded to the Oη of Tyr440 and the Oδ of Asn219.

Modeling of a [4Fe-4S] cluster

So far, four crystal structures of radical SAM enzymes with bound SAM are available from the Protein Data Bank (PDB): biotin (24) synthase (BioB; PDB ID 1R3O)[19], HemN (PDB ID 1OLT)[20], MoaA (PDB ID 2FB3)[21] and LAM (PDB ID 2A5H)[22]. Each displays a $(\beta\alpha)_8$ barrel or modified β-barrel fold in which SAM is ligated through its amino and carboxylate groups to a [4Fe-4S] cluster. When these four radical SAM enzymes are superimposed, the [4Fe-4S] clusters and SAM binding sites overlap well. Even though the CX_3CX_2C motifs of these enzymes are located near the N terminus and the CX_2CX_4C motif of HMP-P synthase is located near the C terminus, we superimposed the structure of biotin synthase onto HMP-P synthase in order to predict the location of its [4Fe-4S] site. After superposition, the [4Fe-4S] cluster is located in an open part of the HMP-P synthase active site with very few bad contacts between either the cluster or the amino acid residues of the cluster binding loop. Notably, the [4Fe-4S] cluster and its binding loop are juxtaposed with the final C-terminal residue visible in the HMP-P synthase X-ray structure. This final residue immediately precedes the conserved CX_2CX_4C motif of HMP-P synthase. Therefore, we used the biotin synthase backbone as a guide for threading the residues of the putative HMP-P synthase [4Fe-4S] binding domain. Following manual adjustment and energy minimization, the modeled [4Fe-4S] binding domain showed no bad contacts and had good geometry with the cysteine residues Cys561, Cys564 and Cys569, which provide ligands for the iron atoms (**Fig. 4b,c**). Furthermore, the modeled cluster positions the SAM molecule near the ribose ring of the substrate analog IMR in an orientation from which the adenosyl radical could abstract a hydrogen atom from the substrate ribose or from the protein to generate the organic radical shown in **Figure 3b**.

Structural similarities to other proteins

A DALI search (http://www.ebi.ac.uk/dali/) using the entire HMP-P synthase structure as the query failed to identify the radical SAM enzymes or any other structural homologs. However, a DALI search using only the $(\beta\alpha)_8$ barrel domain (residues 214–510) identified three of the radical SAM enzymes as structural homologs (**Supplementary Table 2** online). Of these, BioB gave the highest *Z*-score (13.0), and LAM and HemN gave DALI *Z*-scores of 5.9 and 5.1, respectively.

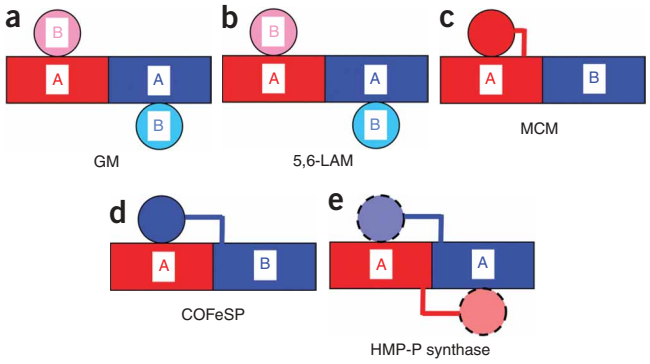

Figure 5 Cartoons depicting the domain assemblies of cobalamin-dependent enzymes with HMP-P synthase–like protomers and dimer interfaces. Each chain within a molecule is color coded differently. (**a**) Glutamate mutase (GM) from *C. sticklandii*. GM contains two identical catalytic subunits and two identical AdoCbl binding subunits, which cap the catalytic domains, forming an $(AB)_2$ heterotetramer. (**b**) Lysine 5,6-amino mutase. 5,6-LAM forms an $(AB)_2$ heterotetramer with an assembly similar to that of GM. (**c**) Methylmalonyl coenzyme A mutase from *P. shermanii*. The catalytic and AdoCbl binding domains are fused (A). The blue subunit (B) does not contain a catalytic site. (**d**) Carbon monoxide dehydrogenase corrinoid/iron-sulfur protein. The blue subunit contains a $(\beta\alpha)_8$ domain (B), with no catalytic site, fused to an MeCbl binding domain, which caps the active site of the catalytic domain (A). (**e**) HMP-P synthase from *C. crescentus*. HMP synthase is a homodimer. The $(\beta\alpha)_8$ core domain is fused to the predicted [4Fe-4S] binding domain. This domain is disordered in the crystal structure, but the final ordered residues extend into the active site of the adjacent protomer and are preceded by a three-helix bundle that anchors the C terminus to the adjacent protomer.

Biotin synthase has a conventional $(\beta\alpha)_8$ barrel, whereas LAM and HemN have modified barrels referred to as β-crescents, which probably accounts for the differences in *Z*-scores.

In addition to the radical SAM enzymes described above, the DALI search identified a group of adenosylcobalamin (AdoCbl, 25) radical enzymes that are also structural homologs with *Z*-scores ranging from 16.0 to 21.0 (**Supplementary Table 2**). The top two DALI *Z*-scores correspond to glutamate (26) mutase from *Clostridium cochlearium*[23] (PDB ID 1CB7) and lysine (27) 5,6-aminomutase from *Clostridium sticklandii*[24] (5,6-LAM, PDB ID 1XRS). Furthermore, glutamate mutase (**Fig. 5a**) and LAM (**Fig. 5b**) have tandem $(\beta\alpha)_8$ barrels that superimpose well on the HMP-P synthase homodimer. The catalytic domain (A) and the AdoCbl binding domain (B) are separate chains generating an $(AB)_2$ heterotetramer.

The top ten matches also include three other tandem $(\beta\alpha)_8$ barrel structures that superimpose well with the HMP-P dimer: a methionine (28) synthase domain from *Thermotoga maritima* (MetH, PDB ID 1Q7M, $Z = 18.2$)[25], methylmalonyl coenzyme A (29) mutase from *Propionibacterium shermanii* (MCM, PDB ID 1REQ, $Z = 17.3$)[26] and carbon monoxide dehydrogenase corrinoid/iron-sulfur protein ($Z = 16.0$) (CoFeSP, PDB ID 2H9A, $Z = 16.0$)[27]. MCM (**Fig. 5c**) displays nonequivalent $(\beta\alpha)_8$ barrels, only one of which contains an active site. Fused to this domain is an AdoCbl binding domain that is positioned near the active site. CoFeSP (**Fig. 5d**), which uses methylcobalamin (MeCbl, 30) as a cosubstrate, also displays nonequivalent $(\beta\alpha)_8$ barrels with one active site. The MeCbl binding domain is fused to the noncatalytic domain and positioned near the active site of the catalytic domain. Though there are structures of all domains of MetH, there is no intact structure that shows the relationship between the MeCbl binding domains and the $(\beta\alpha)_8$ barrel substrate binding domains.

DISCUSSION

The bacterial HMP-P synthase catalyzes a rearrangement reaction of AIR to form the pyrimidine moiety of thiamine (**Fig. 1b**). Our initial attempts at reconstituting this reaction in a cell-free extract from an *E. coli* HMP-P synthase overexpression strain yielded very low activity. However, this activity was sufficient to complete an *in vitro* labeling study that identified the origin of most of the atoms of HMP as well as the cofactor requirements of the reaction[7]. The reaction showed an absolute requirement for AIR and was enhanced by SAM and reduced nicotinamide (31), and by the addition of cell-free extract from wild-type *E. coli*.

Active enzyme was obtained by treating *E. coli* cell-free extract containing *C. crescentus* HMP-P synthase with Fe(II) and sulfide under anaerobic conditions followed by anaerobic purification by Ni-NTA chromatography. Similar preparations were obtained by overexpressing HMP-P synthase in an *E. coli* strain that also overexpressed the enzymes required for iron-sulfur cluster biosynthesis. Our efforts to reconstitute active HMP-P synthase were greatly facilitated by the availability of a highly sensitive assay using the other thiamine biosynthetic enzymes needed to convert minute amounts of biosynthesized HMP-P to the intensely fluorescent thiochrome phosphate (**Supplementary Fig. 1b**). The use of this assay to optimize the reconstitution resulted in a biochemically defined HMP-P synthesizing system, requiring only AIR and SAM as the substrates, dithionite as the reducing agent and purified iron-sulfur cluster–containing HMP-P synthase. Although the thiochrome assay does not identify the phosphorylation state of the pyrimidine as the phosphate is lost during thiamine phosphate formation, the optimized reconstitution yielded sufficient product for direct HPLC analysis. In this way, the products of the reaction were identified as HMP-P and 5-dAdo. Currently, this system is not catalytic, and the observed yield of HMP-P production is ~10% (chemical reconstitution) or ~50% (*in vivo* reconstitution) with respect to the enzyme added. Incorporation of excess AIR or SAM did not result in any further enhancement of the product yield. However, this reconstitution of active, purified HMP-P synthase is an important advance. It has enabled us to experimentally demonstrate that HMP-P synthase is a radical SAM enzyme and to characterize the [4Fe-4S] cluster using Mössbauer and EPR spectroscopies, and it also opens up the system for detailed mechanistic characterization.

The large radical SAM superfamily was established on the basis of a common CX_3CX_2C sequence using bioinformatics[12]. The conserved cysteine residues are usually located near the N terminus of the protein, but they are occasionally found near the middle; however, the [4Fe-4S] cluster and SAM are in the same place in the known structures. HMP-P synthase was not originally included in this superfamily. The observation of a different conserved cysteine pattern near the C terminus and the prediction that these residues form a separate swapped SAM binding domain, together with the reconstitution of the [4Fe-4S] cluster and the observation of 5′-deoxyadenosine as a product, demonstrate that HMP-P synthase is a new member of the superfamily.

Sequence alignments of HMP-P synthase orthologs reveal that HMP-P synthases from anaerobes are shorter than those from aerobes—the former may lack up to 130 residues in the N terminus and 30 residues in the C terminus. The $(\beta\alpha)_8$ core domain appears to be highly conserved, and the three cysteine residues near the C terminus are absolutely conserved (**Supplementary Fig. 6a**). In anaerobic organisms, the [4Fe-4S] binding loop is followed by only about 20 residues, whereas in aerobic organisms there are about 50 residues. Likewise, the N-terminal domains, which fold over the bottom (N-terminal end) and side of the $(\beta\alpha)_8$ barrel, contain only about

70 residues for anaerobes and about 210 residues for aerobes, which suggests that the extra residues provide protection for the oxygen-sensitive iron-sulfur cluster[13].

The AdoCbl radical enzyme superfamily and radical SAM superfamily are functionally related in that both use a 5′-deoxyadenosyl radical for carrying out molecular rearrangements; this suggests the possibility of an evolutionary relationship[28]. Structural evidence for an evolutionary relationship was provided by the observation that both superfamilies use $(\beta\alpha)_8$ barrels[29]. The prediction of a separate SAM binding domain for HMP-P synthase and a common tandem $(\beta\alpha)_8$ barrel interface provides further structural evidence for such a link between these two superfamilies (**Fig. 5**). This might have occurred through a common ancestor with separate cofactor and catalytic subunits in which a SAM binding domain and a AdoCbl binding domain could exchange, followed by gene fusions that eventually committed the enzymes to one or the other of the cofactors.

The structural and biochemical studies described here demonstrate that the bacterial HMP-P synthase is a radical SAM enzyme. In these enzymes, a reduced [4Fe-4S] cluster reduces SAM to give the adenosyl radical. This radical then participates in the isomerization of AIR to HMP-P. The production of 5-dAdo as a product of the reaction suggests that the hydrogen atom abstracted by 5-dAdo is not returned to the product. Aside from the results of the labeling experiments (**Fig. 1b**), we do not yet know the mechanism of this novel rearrangement reaction. Because of the large number of possibilities, we will refrain from proposing a mechanism until the catalytic competence of the protein-bound radical has been established, the site of initial hydrogen atom abstraction has been identified and the fates of the ribose C1′ and C3′ carbon atoms, both of which are absent in HMP-P, have been determined.

Note added in proof: While this paper was under review, the successful reconstitution of the ThiC-catalyzed reaction was reported[47].

METHODS

Expression and purification of *C. crescentus* HMP-P synthase. The gene coding for HMP-P synthase was amplified by PCR from *C. crescentus* genomic DNA and cloned into the expression vector pDESTF1 (Invitrogen). The plasmid was transformed into the *E. coli* Rosetta (DE3) expression strain (Novagen), which contained a second plasmid to supplement the *argU*, *argW*, *glyT*, *IleX*, *leuW*, *metT*, *proL*, *thrT*, *thrU* and *tyrU* tRNAs. Expression of HMP-P synthase was induced at an optical density at 600 nm (OD_{600}) of 0.6–0.8 with 0.5 mM isopropyl-β-D-thiogalactopyranoside (32), and incubation was continued overnight at 298 K. Cells were harvested by centrifugation at 5,000 r.p.m. for 10 min and kept at –80 °C. Purification of the selenomethionine (SeMet, 33)-substituted protein is described in the **Supplementary Methods** online.

Purification of iron-sulfur cluster–reconstituted HMP-P synthase. 3.5 ml of the filtered clarified lysate on ice was transferred into the glove box for reconstitution of the iron-sulfur cluster under strictly anaerobic conditions. Freshly prepared 500 mM DTT stock solution was added to obtain a final concentration of 10 mM. Ferrous ammonium sulfate was added to a final concentration of 10 mM in small aliquots, ensuring thorough mixing. Sodium sulfide was then added to the same final concentration in a similar fashion. The mixture was allowed to incubate on ice for 30 min, and then 3 ml of this solution, dark in color, was loaded onto a Bio-Rad 10-DG desalting column pre-equilibrated with 200 mM Tris-HCl buffer, pH 7.6, containing 4 mM $MgCl_2$ and 1 mM DTT. Later, it was further subjected to Ni-NTA affinity purification as described in the **Supplementary Methods**.

HMP-P biosynthesis reconstitution assay. Assays were set up in a glovebox under strictly anaerobic conditions. A typical assay mixture contained 800 μM SAM, 400 μM AIR, 10 mM dithionite and 200 μl of protein (purified or in cell-free extract). The enzyme concentration varied between 0.8 and 1.2 mM among preparations for purified HMP-P synthase. Total protein concentration in cell-free extract varied between 35 and 40 mg ml^{-1}. Products were detected directly or with a thiochrome assay as described in the **Supplementary Methods**.

Mössbauer and EPR spectroscopies. Mössbauer spectra were recorded on a spectrometer (WEB research) operating in the constant acceleration mode in a transmission geometry. Spectra were recorded with the temperature of the sample maintained at 4.2 K in an externally applied magnetic field of 53 mT oriented parallel to the γ beam. The quoted isomer shifts are relative to the centroid of the spectrum of a foil of α-Fe metal at room temperature (295 K). Data analysis was performed using WMOSS (WEB research).

Low-temperature X-band EPR spectra were recorded in perpendicular mode on a Bruker Elexsys E-560 instrument. Sample temperature was maintained with an ITC503S temperature controller and an ESR900 liquid helium cryostat, both from Oxford Instruments. Samples, which contained 500 μM HMP-P synthase in a total volume of 500 μl, were loaded into EPR tubes and frozen in liquid N_2 inside of a Coy anaerobic chamber.

Crystallization of HMP-P synthase. The SeMet HMP-P synthase–HMP crystals were grown using the sitting drop vapor diffusion method at 298 K by mixing 5.0 μl of the protein solution ($\sim$10 mg ml^{-1}) with 4.0 μl of a well solution (30% polyethylene glycol (PEG) 4000, 100 mM Tris-HCl, pH 8.2, 200 mM Li_2SO_4, 2.0 mM DTT) and 1.0 μl of 100 mM HMP. Plate crystals appeared within 3 d and took 1 to 2 weeks to reach their maximum size of 0.05 mm × 0.1 mm × 0.01 mm. The crystals were monoclinic, space group $P2_1$, with unit cell dimensions a = 63.3 Å, b = 103.4 Å, c = 95.4 Å and β = 91.6°. Assuming two HMP-P synthase molecules of 68 kDa in the asymmetric unit, the Matthews coefficient V_M is 2.29 $Å^3$ Da^{-1}, which corresponds to a solvent content of 46.4% (ref. 30). For cryoprotection, the crystals were transferred to a cryoprotectant containing 30% PEG4000, 100 mM Tris-HCl, pH 8.2, 200 mM Li_2SO_4, 2.0 mM DTT and 15% glycerol (v/v), immediately frozen in the cryostream, and stored under liquid nitrogen before data collection. Crystallization of the additional complexes is described in the **Supplementary Methods**.

X-ray data collection and processing. All of the HMP-P synthase X-ray diffraction data were collected at the Northeastern Collaborative Access Team (NE-CAT) beamlines 24-ID-C and 24-ID-E of the Advanced Photon Source (APS) at a wavelength of 0.97918 Å. The data were integrated and scaled using HKL2000 (ref. 31). Data collection details are described in the **Supplementary Methods**. The data collection statistics are summarized in **Supplementary Table 1**.

Structure determination and refinement. The crystal structure of HMP-P synthase from *C. crescentus* was solved by single wavelength anomalous diffraction (SAD) methods at 2.8 Å resolution using SeMet-substituted HMP-P–HMP crystal. Selenium sites were located using ShelxD[32,33] and were refined with MLPHARE[34]. RESOLVE[35] was used for initial model building, and the model was completed using O[36] and Coot[37]. Structure refinement was performed using CNS[38]. The model quality was assessed at intervals with PROCHECK[39]. The structures of the complexes were refined at 2.0 Å resolution. Additional details are provided in the **Supplementary Methods**. For the HMP-P synthase structures, 84.8% to 88.9% of the nonglycine residues are in the most favored region of the Ramachandran plot, with no residue in the disallowed region. The final refinement statistics are shown in **Supplementary Table 1**.

Structural analysis. Structure-based sequence alignments were done either using the protein structure comparison server SSM[40] at the European Bioformatics Institute or using LSQKAB[41] of the CCP4 suite. The sequence alignment figure was prepared with ESPript[42]. The Protein-Protein Interaction Server[43,44] was used to analyze protein-protein interfaces for accessible surface area, hydrogen bonds and salt bridges. Figures were prepared with PyMOL[45] and CCP4mg[46].

Synthesis of IMR. The chemical synthesis of IMR is outlined in **Supplementary Fig. 7c** and described in the **Supplementary Methods**.

Accession codes. Protein Data Bank: The coordinates for HMP-P synthase–HMP, HMP-P synthase–HMP-P and HMP-P synthase–IMR have been deposited under the accession codes 3EPM, 3EPO and 3EPN, respectively. The crystal structures of radical SAM enzymes with bound SAM were deposited as part of previous studies: biotin synthase (PDB ID 1R3O)[19], HemN (PDB ID 1OLT)[20], MoaA (PDB ID 2FB3)[21] and LAM (PDB ID 2A5H)[22]. The following structures were also deposited as part of previous studies: glutamate mutase from *C. cochlearium*[23] (PDB ID 1CB7), lysine 5,6-aminomutase from *C. sticklandii*[24] (PDB ID 1XRS), a methionine synthase domain from *T. maritima* (PDB ID 1Q7M)[25], methylmalonyl coenzyme A mutase from *P. shermanii* (PDB ID 1REQ)[26] and carbon monoxide dehydrogenase corrinoid/iron-sulfur protein (PDB ID 2H9A)[27].

Note: Supplementary information and chemical compound information is available on the Nature Chemical Biology website.

ACKNOWLEDGMENTS

We thank NE-CAT beamline 24-ID-C, supported by US National Institutes of Health grant RR15301, for the use of beam time. We thank C. Kinsland (Cornell University Protein Facility) for the preparation of the HMP-P synthase overexpression plasmid and L. Kinsland for assistance in the preparation of this manuscript. This work was supported by US National Institutes of Health grants DK44083 (T.P.B.), GM63847 (S.J.B.) and DK67081 (S.E.E.), the Beckman Foundation (Young Investigator Award to C.K.) and the Dreyfus Foundation (Camille Dreyfus Teacher Scholar Award to C.K.). S.E.E. is indebted to the W.M. Keck Foundation and the Lucille P. Markey Charitable Trust.

AUTHOR CONTRIBUTIONS

A.C. performed all biochemical studies. Y.L. and Y.Z. performed all crystallographic studies. T.L.G. assisted in protein purification and EPR spectroscopy. M.L. recorded and analyzed Mössbauer spectra. C.K. and S.J.B. directed the EPR and Mössbauer studies, T.P.B. directed the biochemical studies and S.E.E. directed the crystallographic studies.

Published online at http://www.nature.com/naturechemicalbiology/
Reprints and permissions information is available online at http://npg.nature.com/reprintsandpermissions/

1. Begley, T.P. *et al.* Thiamin biosynthesis in prokaryotes. *Arch. Microbiol.* **171**, 293–300 (1999).
2. Settembre, E., Begley, T.P. & Ealick, S.E. Structural biology of enzymes of the thiamin biosynthesis pathway. *Curr. Opin. Struct. Biol.* **13**, 739–747 (2003).
3. Chatterjee, A., Jurgenson, C.T., Schroeder, F.C., Ealick, S.E. & Begley, T.P. Thiamin biosynthesis in eukaryotes: characterization of the enzyme-bound product of thiazole synthase from *Saccharomyces cerevisiae* and its implications in thiazole biosynthesis. *J. Am. Chem. Soc.* **128**, 7158–7159 (2006).
4. Chatterjee, A., Jurgenson, C.T., Schroeder, F.C., Ealick, S.E. & Begley, T.P. Biosynthesis of thiamin thiazole in eukaryotes: conversion of NAD to an advanced intermediate. *J. Am. Chem. Soc.* **129**, 2914–2922 (2007).
5. Jurgenson, C.T., Chatterjee, A., Begley, T.P. & Ealick, S.E. Structural insights into the function of the thiamin biosynthetic enzyme Thi4 from *Saccharomyces cerevisiae*. *Biochemistry* **45**, 11061–11070 (2006).
6. Kriek, M. *et al.* Thiazole synthase from *Escherichia coli*: an investigation of the substates and purified proteins required for activity *in vitro*. *J. Biol. Chem.* **282**, 17413–17423 (2007).
7. Lawhorn, B.G., Mehl, R.A. & Begley, T.P. Biosynthesis of the thiamin pyrimidine: the reconstitution of a remarkable rearrangement reaction. *Org. Biomol. Chem.* **2**, 2538–2546 (2004).
8. Newell, P.C. & Tucker, R.G. Biosynthesis of the pyrimidine moiety of thiamine. A new route of pyrimidine biosynthesis involving purine intermediates. *Biochem. J.* **106**, 279–287 (1968).
9. Zeidler, J., Sayer, B.G. & Spenser, I.D. Biosynthesis of vitamin B1 in yeast. Derivation of the pyrimidine unit from pyridoxine and histidine. Intermediacy of urocanic acid. *J. Am. Chem. Soc.* **125**, 13094–13105 (2003).
10. Frey, P.A. & Booker, S.J. Radical mechanisms of *S*-adenosylmethionine-dependent enzymes. *Adv. Protein Chem.* **58**, 1–45 (2001).
11. Wang, S.C. & Frey, P.A. *S*-adenosylmethionine as an oxidant: the radical SAM superfamily. *Trends Biochem. Sci.* **32**, 101–110 (2007).
12. Sofia, H.J., Chen, G., Hetzler, B.G., Reyes-Spindola, J.F. & Miller, N.E. Radical SAM, a novel protein superfamily linking unresolved steps in familiar biosynthetic pathways with radical mechanisms: functional characterization using new analysis and information visualization methods. *Nucleic Acids Res.* **29**, 1097–1106 (2001).
13. Dougherty, M.J. & Downs, D.M. A connection between iron-sulfur cluster metabolism and the biosynthesis of 4-amino-5-hydroxymethyl-2-methylpyrimidine pyrophosphate in *Salmonella enterica*. *Microbiology* **152**, 2345–2353 (2006).
14. Raschke, M. *et al.* Vitamin B1 biosynthesis in plants requires the essential iron sulfur cluster protein, THIC. *Proc. Natl. Acad. Sci. USA* **104**, 19637–19642 (2007).
15. Reddick, J.J., Nicewonger, R. & Begley, T.P. Mechanistic studies on thiamin phosphate synthase: evidence for a dissociative mechanism. *Biochemistry* **40**, 10095–10102 (2001).
16. Park, J.-H., Burns, K., Kinsland, C. & Begley, T.P. Characterization of two kinases involved in thiamine pyrophosphate and pyridoxal phosphate biosynthesis in *Bacillus subtilis*: 4-amino-5-hydroxymethyl-2-methylpyrimidine kinase and pyridoxal kinase. *J. Bacteriol.* **186**, 1571–1573 (2004).
17. Cicchillo, R.M. *et al. Escherichia coli* lipoyl synthase binds two distinct [4Fe-4S] clusters per polypeptide. *Biochemistry* **43**, 11770–11781 (2004).
18. Münck, E. in *Physical Methods in Bioinorganic Chemistry* (ed. Que, L. Jr.) 287–319 (University Science Books, Sausalito, California, USA, 2000).
19. Vallazza, M. *et al.* First look at RNA in L-configuration. *Acta Crystallogr. D Biol. Crystallogr.* **60**, 1–7 (2004).
20. Layer, G., Moser, J., Heinz, D.W., Jahn, D. & Schubert, W.D. Crystal structure of coproporphyrinogen III oxidase reveals cofactor geometry of radical SAM enzymes. *EMBO J.* **22**, 6214–6224 (2003).
21. Hanzelmann, P. & Schindelin, H. Crystal structure of the *S*-adenosylmethionine-dependent enzyme MoaA and its implications for molybdenum cofactor deficiency in humans. *Proc. Natl. Acad. Sci. USA* **101**, 12870–12875 (2004).
22. Lepore, B.W., Ruzicka, F.J., Frey, P.A. & Ringe, D. The x-ray crystal structure of lysine-2,3-aminomutase from *Clostridium subterminale*. *Proc. Natl. Acad. Sci. USA* **102**, 13819–13824 (2005).
23. Reitzer, R. *et al.* Glutamate mutase from *Clostridium cochlearium*: the structure of a coenzyme B12-dependent enzyme provides new mechanistic insights. *Structure* **7**, 891–902 (1999).
24. Berkovitch, F. *et al.* A locking mechanism preventing radical damage in the absence of substrate, as revealed by the x-ray structure of lysine 5,6-aminomutase. *Proc. Natl. Acad. Sci. USA* **101**, 15870–15875 (2004).
25. Evans, J.C. *et al.* Structures of the N-terminal modules imply large domain motions during catalysis by methionine synthase. *Proc. Natl. Acad. Sci. USA* **101**, 3729–3736 (2004).
26. Mancia, F. *et al.* How coenzyme B12 radicals are generated: the crystal structure of methylmalonyl-coenzyme A mutase at 2 Å resolution. *Structure* **4**, 339–350 (1996).
27. Svetlitchnaia, T., Svetlitchnyi, V., Meyer, O. & Dobbek, H. Structural insights into methyltransfer reactions of a corrinoid iron-sulfur protein involved in acetyl-CoA synthesis. *Proc. Natl. Acad. Sci. USA* **103**, 14331–14336 (2006).
28. Frey, P.A. Radical mechanisms of enzymatic catalysis. *Annu. Rev. Biochem.* **70**, 121–148 (2001).
29. Berkovitch, F., Nicolet, Y., Wan, J.T., Jarrett, J.T. & Drennan, C.L. Crystal structure of biotin synthase, an *S*-adenosylmethionine-dependent radical enzyme. *Science* **303**, 76–79 (2004).
30. Matthews, B.W. Solvent content of protein crystals. *J. Mol. Biol.* **33**, 491–497 (1968).
31. Otwinowski, Z. & Minor, W. Processing of X-ray diffraction data collected in oscillation mode. *Methods Enzymol.* **276**, 307–326 (1997).
32. Schneider, T.R. & Sheldrick, G.M. Substructure solution with SHELXD. *Acta Crystallogr. D Biol. Crystallogr.* **58**, 1772–1779 (2002).
33. Uson, I. & Sheldrick, G.M. Advances in direct methods for protein crystallography. *Curr. Opin. Struct. Biol.* **9**, 643–648 (1999).
34. Otwinowski, Z. in *CCP4 Proceedings* (eds. Wolf, W., Evans, P.R. & Leslie, A.G.W.) 80–88 (SERC Daresbury Laboratory, Warrington, UK, 1991).
35. Terwilliger, T.C. Maximum-likelihood density modification. *Acta Crystallogr. D Biol. Crystallogr.* **56**, 965–972 (2000).
36. Jones, T.A., Zou, J.-Y., Cowan, S.W. & Kjeldgaard, M. Improved methods for the building of protein models in electron density maps and the location of errors in these models. *Acta Crystallogr. A* **47**, 110–119 (1991).
37. Emsley, P. & Cowtan, K. Coot: model-building tools for molecular graphics. *Acta Crystallogr. D Biol. Crystallogr.* **60**, 2126–2132 (2004).
38. Brünger, A.T. *et al.* Crystallography & NMR system: a new software suite for macromolecular structure determination. *Acta Crystallogr. D Biol. Crystallogr.* **54**, 905–921 (1998).
39. Laskowski, R.A., Moss, D.S. & Thornton, J.M. Main-chain bond lengths and bond angles in protein structures. *J. Mol. Biol.* **231**, 1049–1067 (1993).
40. Krissinel, E. & Henrick, K. Secondary-structure matching (SSM), a new tool for fast protein structure alignment in three dimensions. *Acta Crystallogr. D Biol. Crystallogr.* **60**, 2256–2268 (2004).
41. Kabsch, W., Kabsch, H. & Eisenberg, D. Packing in a new crystalline form of glutamine synthetase from *Escherichia coli*. *J. Mol. Biol.* **100**, 283–291 (1976).
42. Gouet, P., Courcelle, E., Stuart, D.I. & Metoz, F. ESPript: analysis of multiple sequence alignments in PostScript. *Bioinformatics* **15**, 305–308 (1999).
43. Jones, S. & Thornton, J.M. Protein-protein interactions: a review of protein dimer structures. *Prog. Biophys. Mol. Biol.* **63**, 31–65 (1995).
44. Jones, S. & Thornton, J.M. Principles of protein-protein interactions. *Proc. Natl. Acad. Sci. USA* **93**, 13–20 (1996).
45. DeLano, W.L. *The PyMOL Molecular Graphics System* (DeLano Scientific, San Carlos, California, USA, 2002).
46. Potterton, E., McNicholas, S., Krissinel, E., Cowtan, K. & Noble, M. The CCP4 molecular-graphics project. *Acta Crystallogr. D Biol. Crystallogr.* **58**, 1955–1957 (2002).
47. Martinez-Gomez, N.C. & Downs, D.M. ThiC is an [Fe-S] cluster protein that requires AdoMet to generate the 4-amino-5-hydroxymethyl-2-methylpyrimidine moiety in thiamin synthesis. *Biochemistry* **47**, 9054–9056 (2008).